

Low-temperature statistical mechanics of the Quantizer problem: fast quenching and equilibrium cooling of the three-dimensional Voronoi Liquid

Tobias M. Hain,^{1,2,3} Michael A. Klatt,^{4,5} and Gerd E. Schröder-Turk^{3,6,2,7}

¹*Institut für Mathematik, Universität Potsdam, Karl-Liebknecht-Str. 24-25, D-14476 Potsdam OT Golm*

²*Physical Chemistry, Center for Chemistry and Chemical Engineering, Lund University, Lund 22100, Sweden*

³*Murdoch University, College of Science, Health, Engineering and Education, Mathematics and Statistics, 90 South St, Murdoch WA 6150, Australia*

⁴*Department of Physics, Princeton University, Princeton, NJ 08544, USA*

⁵*Present address: Friedrich-Alexander-Universität Erlangen-Nürnberg (FAU), Institut für Theoretische Physik, Staudstr. 7, 91058 Erlangen, Germany, and Department of Experimental Physics, Saarland University, Campus E2 9, 66123 Saarbrücken, Germany*

⁶*Department of Food Science, University of Copenhagen, Rolighedsvej 26, 1958 Frederiksberg C, Denmark*

⁷*Email for correspondence: g.schroeder-turk@murdoch.edu.au*

(Dated: 15 December 2020)

The Quantizer problem is a tessellation optimization problem where point configurations are identified such that the Voronoi cells minimize the second moment of the volume distribution. While the ground state (optimal state) in 3D is almost certainly the body-centered cubic lattice, disordered and effectively hyperuniform states with energies very close to the ground state exist that result as stable states in an evolution through the geometric Lloyd’s algorithm [Klatt *et al.* Nat. Commun., 10, 811 (2019)]. When considered as a statistical mechanics problem at finite temperature, the same system has been termed the ‘Voronoi Liquid’ by [Ruscher *et al.* EPL 112, 66003 (2015)]. Here we investigate the cooling behaviour of the Voronoi liquid with a particular view to the stability of the effectively hyperuniform disordered state. As a confirmation of the results by Ruscher *et al.*, we observe, by both molecular dynamics and Monte Carlo simulations, that upon slow quasi-static equilibrium cooling, the Voronoi liquid crystallizes from a disordered configuration into the body-centered cubic configuration. By contrast, upon sufficiently fast non-equilibrium cooling (and not just in the limit of a maximally fast *quench*) the Voronoi liquid adopts similar states as the effectively hyperuniform inherent structures identified by Klatt *et al.* and prevents the ordering transition into a BCC ordered structure. This result is in line with the geometric intuition that the geometric Lloyd’s algorithm corresponds to a type of fast quench.

The following article has been accepted by the Journal of Chemical Physics. After it is published, it will be found at <https://doi.org/10.1063/5.0029301>.

I. INTRODUCTION

Geometric optimization problems of tessellations search for partitions of space into cells with certain optimal geometric properties. Often these geometric properties can be expressed as energy functionals, so that the global optimum corresponds to the ground state of a physical system. Thus, the geometric optimization problem relates fundamental questions in mathematics and physics. Famous examples in three dimensions (3D) are the Kelvin problem^{1,2} (that is, the search for a tessellation with equal volume cells that have the least surface area) and the Kepler problem³ (that is, the search for cells with the highest packing fraction of impenetrable spheres).

While global optima correspond to ground states of physical systems, local optima correspond to inherent structures (that is, local minima of a complex energy landscapes). At low-temperature, an equilibrium system will typically be different from a non-equilibrium state that is reached by a quench. Such a fast non-equilibrium cooling often leads to glass-like, highly disordered states. There are, however, also potentials that exhibit disordered ground states and that are hence often highly degenerate. Examples include stealthy po-

tentials, where the ground states suppress single scattering up a finite wave number K . The potential suppresses density fluctuations at large scales⁴⁻⁶, and as a rigorous consequence, the ground state does not allow for arbitrarily large holes^{7,8}. Another class of examples are models of “perfect glass”, which involve up to four-body interactions and do not allow for crystalline ground states (but only disordered configurations)⁹. Disordered ground states have also been empirically found in vertex models that optimize the isoperimetric ratios of cells (modelling biological tissues)^{10,11}.

More generally, we are here interested in models with energy landscapes that allow for metastable amorphous states that have energies close to the crystalline ground state.

The geometric optimization problem that we consider here is the *Quantizer problem*¹²⁻¹⁷, that is, we optimize the second moment of inertia of each cell. Intuitively speaking, the optimization prefers equal-volume cells with “sphere-like” shapes. It is a prominent problem in computer science, where it is applied for example in compression algorithms¹⁸ or mesh generation of two-dimensional manifolds¹⁹. In recent years, the Quantizer problem has attracted attention in physics since it relates to a many-body interaction that results in surprising physical and geometrical properties²⁰⁻²³.

Given a configuration of N points in Euclidean space, the Voronoi quantizer (or Voronoi tessellation) assigns to each point \mathbf{z}_i a cell C_i that contains all sites in space that are closer to that point than to any other point in point pattern¹⁵. The

cells subdivide space without overlap. The Quantizer energy E_i of a single cell C_i is then defined as the moment of inertia of the cell interpreted as a solid object and measured with respect to the Voronoi center \mathbf{z}_i ^{17,20,21}. More precisely, the total energy E of the system is the sum of the cell energies E_i , defined as follows:

$$E = \sum_{i=1}^N E_i \quad \text{with} \quad E_i = \frac{\gamma}{2} \int_{C_i} \|\mathbf{x} - \mathbf{z}_i\|^2 d\mathbf{x}. \quad (1)$$

where γ is a coefficient to set the dimension of eq. 1 to an energy and N is the number of points (respectively cells).

The Quantizer problem is defined for a fixed number of points N . Note that this formulation of the Quantizer energy is extensive, in contrast to the intensive *Quantizer error*, which is the rescaled sum of all single cell energies (see²³ for more details). The energy functional can also be expressed by the Minkowski tensors²⁴ of the cell C_i (see below)²³. The Quantizer energy functional assigns an energy to each point configuration in Euclidean space. The Quantizer problem in computer science has thus been reformulated as a ground state problem in statistical physics²⁰.

In 3D, the conjectured optimal solution of the Quantizer problem, that is, the ground state, is the body-centered cubic (BCC) lattice¹⁴. It is closely related Kelvin's conjectured equal-volume cells with least surface area^{2,25}. A conjecture that was later disproven by the counterexample of Weaire and Phelan¹. The proof of the Kepler conjecture (that no packing of monodisperse spheres has a larger packing fraction than the face-centered cubic (FCC) packing) reformulates the problem as an optimization problem of tessellations (including Voronoi cells)³.

Here, we are interested in disordered inherent structures with energies close to that of the ground state. Following the approach from Ruscher, Baschnagel, and Farago²¹, we study both equilibrium and non-equilibrium dynamics of a many-particle system whose energy is defined by a rescaled Quantizer energy, that is, a geometrically driven particle system with many-body interactions. Our focus is on order/disorder transitions, that is, on the degree of structural order and disorder of different states and how it changes during melting, slow cooling, or a quench.

Ruscher *et al.* studied in detail this many-particle system from a thermodynamic point of view^{21,22,26} and found intriguing physical behavior like an anomalous sound attenuation²⁷. They named the system the *Voronoi liquid*. The distinct difference to well-established model systems such as the Lennard-Jones fluid is that the interactions in the Voronoi liquid are intrinsically many-body. Ruscher, Baschnagel, and Farago²¹ report theoretical considerations as well as molecular dynamics (MD) simulations that show that the Voronoi liquid in many ways behave similar to an ordinary fluid, including a scaling law for its free energy and derivated quantities as well as dynamic and structural properties. Furthermore a melting and freezing transition when heating and cooling the system are found, showing a metastable state with a hysteresis and under and overcooled states²². Ruscher *et al.* studied the Voronoi liquid as a model glass former where crystallization is prevented by the integration of a term correspond-

ing to bidispersity^{26,28}. Their work without the polydispersity term²¹, and the results of this paper, show that the system without polydispersity and defined by eq. 1 shows a conventional order/disorder transition upon heating or cooling.

Here, we are specifically interested in a better understanding of the inherent structures of the Quantizer problem. In a recent study Klatt *et al.*²³, the so-called Lloyd's algorithm¹³ was applied to a broad range of distinctly different random point patterns to find minimal energy point-configurations. At each step of the algorithm, each point is replaced by the center of mass of its Voronoi cell. Klatt *et al.*²³ showed that upon application of a sufficient number of iterations of the Lloyd's algorithm all initial random point configurations converged to configurations that are amorphous and universal with the same two-point statistics and Minkowski tensors within error bars. Moreover, these final configurations are effectively hyperuniform, that is, they exhibit a strong suppression of large-scale density fluctuations²⁹⁻³¹, as measured by the hyperuniformity index $H = \lim_{k \rightarrow 0} S(k) / \max S(k)$ ^{31,32} with values of $H \lesssim 10^{-4}$. We will here refer to these configurations as the *converged Lloyd state(s)*.

In this article on the Quantizer energy, we study both the equilibrium behavior and non-equilibrium quenches. We thus reproduce and confirm results found by Ruscher, Baschnagel, and Farago²¹. Therefore, we use besides MD also Monte-Carlo (MC) simulations. Moreover, we vary cooling rates to study both crystallization and the freezing in inherent structures. We thus further probe the energy landscape of the Quantizer problem to address the question of the stability of the disordered, effectively hyperuniform states to which the Lloyd's algorithm converges²³. Since we here study in detail the Quantizer problem at finite temperature T , we refer to it as the "Quantizer problem".

This article is structured as followed: in section II we give details about our simulations, in section III we present our results and address the question if a disordered, stable state for the Quantizer problem exists, before we give a summary of this article in section IV.

II. METHODS

Three different numerical methods for the evolution of a point pattern are used in this study: Lloyd's algorithm¹³ is a purely geometric algorithm used to compute gradient-descent-like quenches as previously described and is used in the same way as in Klatt *et al.*²³. Molecular Dynamics (MD) and Monte Carlo (MC) codes are used to determine statistical properties of quasistatic (slowly cooled or heated) systems. Molecular Dynamics is also used to calculate the non-equilibrium evolution of the system when it is quenched, that is, with fast cooling rates.

Throughout this article we will use reduced units. The unit of length is $\lambda = \rho^{-1/3}$, where ρ is the number density. Thus, we choose $\rho = 1$. Each sample contains $N = 2000$ particles in a cubic simulation box (of side length $2000^{1/3}\lambda \approx 12.6\lambda$) using periodic boundary conditions. The unit of energy is $[E] = \varepsilon = \gamma\lambda^5/1000$, where the factor 1000 is chosen fol-

lowing Ruscher, Baschnagel, and Farago²¹. The unit of temperature is $[T] = \varepsilon/k$, where k is the Boltzmann factor. All particles have the same mass m , which here defines the unit of mass. The arbitrary unit of time for the MD simulation is $[t] = \delta$ (Note that the MC simulation and Lloyd's algorithm have no time scale.)

Monte Carlo method We use a simple single-step Metropolis algorithm³³ implemented in the software package MOCASINNS^{34,35}: a trial move is chosen by selecting a random particle \mathbf{x}_i in the system and move it by a random displacement vector $\Delta\mathbf{x}$. The energy difference ΔE for this potential new configuration is then computed. The probability of accepting this trial move $p(\Delta E)$ is then given by

$$p(\Delta E) = \begin{cases} 1 & \text{for } \Delta E < 0 \\ \exp(-\frac{\Delta E}{kT}) & \text{for } \Delta E \geq 0 \end{cases} \quad (2)$$

for a given system temperature kT . If the trial move is accepted, the particle is left at its new position, if the move is declined it is moved back to its original position. The direction of the random displacement vector $\Delta\mathbf{x}$ is random, its length $\|\mathbf{x}\|$ is chosen such as about half of the trial steps are accepted. This is achieved by checking the acceptance ratio in fixed intervals of Monte Carlo steps, and doubling the step size if the acceptance ratio is higher than 0.65 or cutting it in half for an acceptance ratio smaller than 0.35. A lookup table was created to quickly find an appropriate step size for a given particle number and temperature.

An essential part of this algorithm is the computation of the energy difference. To improve performance, only the energies of the cells affected by the move are recomputed according to eq. (1). This definition of the energy is essentially the second moment of the mass distribution of the cell and thus can be expressed as the trace of the Minkowski Tensor $W_0^{2,0}$: $E = \text{tr} [W_0^{2,0}(C_i)]$. Minkowski Tensors are a comprehensive set of metrics, describing geometric properties of a body^{24,36}.

The computation of the cell energy is carried out in two steps: first the Voronoi cell of a particle is computed using the *voro++* software package³⁷, the coordinates of the vertices and edges are then parsed into KARAMBOLA³⁶, a tool to compute the Minkowski tensors. The cell energy is then obtained by computing $E = \text{tr} [W_0^{2,0}(C_i)]$. The total energy of a system is just the sum of all individual cell energies.

Molecular Dynamics is a method to simulate particle systems by forward integration of Newton's equation of motion $\mathbf{a}_i = \frac{\mathbf{F}_i}{m_i}$ in time for each particle, thus computing the exact trajectory for each constituent. The essential part of each MD code is thus the computation of the force acting on each particle. We follow Ruscher, Baschnagel, and Farago²¹ and define the force on the i -th particle as $\mathbf{F}_i = \gamma\boldsymbol{\tau}_i$, where $\boldsymbol{\tau}_i = V_i \cdot (\mathbf{c}_i - \mathbf{z}_i)$ is the so-called polarisation vector with \mathbf{c}_i being the centroid, \mathbf{z}_i the generator, thus position of the i -th particle, and V_i the volume of the i -th cell. The computation of the position of the cell's centroid as well as its volume is done using the software VORO++³⁷.

A velocity Verlet integrator coupled with a simple Nosé-Hoover thermostat³⁸ was used to integrate the equation of motions. The Nosé-Hoover thermostat adds an additional term

$\frac{Q}{2}s^2 - (f+1)kT_{eq}$ to the Lagrangian of the system to reproduce configurations from the NVT ensemble at a temperature kT . The variable s is a variable associated with the thermostat, f is the number of degrees of freedom of the system, kT_{eq} the temperature of the NVT ensemble and Q determines the time scale of the temperature fluctuations introduced by the thermostat. We implemented the formulation by Martyna, Tobias, and Klein³⁹. In each integration step, time is advanced by a time step Δt and the positions \mathbf{x}_i and velocities $\dot{\mathbf{x}}_i$ of each particle as well as the thermostat variable s and its derivative \dot{s} are updated accordingly.

Lloyd's algorithm is a purely geometric algorithm to minimize the Quantizer energy. It comprises the reposition of a simple step: move the generator of a cell \mathbf{z}_i , thus a particle, to the centroid of its cell \mathbf{c}_i .

A typical simulation run, either MD or MC, would consist of the following steps: first, an initial configuration is initialized with a given particle number N and system size.

Initial configurations can be generated as perfect BCC crystal or as an ideal gas, thus each component of each particle is chosen uniformly random across the simulation box, corresponding to a binomial point process. Furthermore simulation can be initialized with arbitrary point configurations read from simple text files, so a previously saved simulation snapshot can be used as initial configuration.

The next step is to choose a cooling schedule: a temperature step size $k\Delta T$ as well as a number of temperature steps N_{kT} is set. For each temperature a set amount of MD or MC steps, called *relax steps* are performed to get the system to thermodynamic equilibrium. Once these are done, another set of steps, called *measurement steps* are performed and relevant measurements are taken, the most important being the energy and τ order parameter. After these are done, the system temperature is increased by $k\Delta T$. This is repeated until the final number of temperature increments has been added. In our MD simulations, the cooling rate is defined as $\sigma = \frac{k\Delta T}{\#\text{relax steps} \cdot \Delta t}$ and thus has the units of energy over time. For MD or MC quenches, this cooling schedule would simply consist of a single temperature $kT = 0$.

The measurement used to describe structures in this study are essentially the Quantizer energy, the Structure factor $S(k)$ and the τ order metric⁴. The structure factor is essentially the scatter intensity of a structure. For a single snapshot of particles in a cubic box of length L with periodic boundary conditions it is given as^{31,40}

$$S(k) = \frac{1}{N} \left| \sum_{i=1}^N e^{-i\mathbf{k} \cdot \mathbf{x}_i} \right|^2 \quad (3)$$

where the sum runs over all particles in the system, $k = \|\mathbf{k}\|$, and $\mathbf{k} \in \{\frac{2\pi}{L}(h, k, l) : (h, k, l) \in \mathbb{Z}^3\}$.

The τ order metric measures spatial correlations on all length scales and is defined as

$$\tau := \frac{\omega_d}{(2\pi)^d} \int_0^\infty k^{d-1} [S(k) - 1]^2 dk, \quad (4)$$

where, d is the dimension, in our case $d = 3$, ω_d is the surface area of a unit ball in d dimensions ($\omega_3 = 4\pi$) and $S(k)$

the structure factor. For a completely disordered, uncorrelated structure τ vanishes, while it diverges as soon as Bragg peaks appear, i.e. especially for systems with a perfect long range order like crystals. Since this parameter unites a large amount of information into a single scalar value it is prone to mainly two errors: small changes in the structure can cause significant change in magnitude of τ , we estimate this error by computing the standard error of multiple runs with identical parameters to $\Delta\tau_{\text{stat}} = 0.1 - 0.15$, depending on the parameters chosen. Systematic errors caused by the choice of the binning of $S(k)$ as well as an upper integration cutoff k_{max} can not be avoided. By computing the standard deviation of different binnings of a single system we estimate these systematic errors to $\Delta\tau_{\text{sys}} = 0.9$. Combining both statistical and systematic errors, we assume a total error of $\Delta\tau \approx 1$, which is in line with the previous analysis by Klatt *et al.*²³.

A detailed list of the parameters used to generate the data in this article is provided in Appendix VII C. Unless stated otherwise, temperature is quantified by kT with the Boltzmann constant k and has units of energy, $[kT] = \epsilon$. All time steps δt have time unit $[\delta t] = \delta$.

III. RESULTS

Our key results concern the structures obtained by a quench of the system, especially in relation to the converged Lloyd states described by Klatt *et al.*²³. However, we first describe our reproduction of the findings of Ruscher²² of an order/disorder transition encountered upon slow equilibrium melting or cooling. Figures 1 and 2 show our results regarding the order/disorder transition upon slow equilibrium cooling or melting.

Figure 1 shows MD simulations essentially of the same system investigated by Ruscher, Baschnagel, and Farago²¹, Ruscher²² and Ruscher *et al.*²⁷. When a Voronoi liquid of $2 \times 10^3 = 2000$ particles is heated slowly (with a heating rate of $\sigma = 2.5 \times 10^{-4} \epsilon / \delta$) starting from positions on a BCC lattice at $kT = 0.1$, it undergoes an order/disorder transition; at $kT_{\text{melt}} \approx 1.89$, the Voronoi liquid abruptly changes from configurations that represent oscillations around the lattice sites to a configuration with no apparent order. Upon further heating this structure is characterised by the correlations typical for a fluid (for very high temperatures we expect it to converge to an ideal gas). This transition is evident in the energy E as well as in the structural order parameter τ . In our simulations of 48 systems, the transition temperatures vary slightly, with an average of 1.89 and a standard deviation of 0.01. These transition temperatures are close to, but slightly above the observed transition $kT \approx 1.85$ in^{21,22}. Our curves for the structure factor in the liquid phase agree with those from²².

Upon cooling (with the same slow rate as above and starting from an ideal gas configuration at $kT = 2.1$), the system shows the reverse transition from a disordered state to an ordered BCC-like state, at a temperature $kT_{\text{cool}} = 0.96 \pm 0.04$ (again close to but slightly below the temperature $kT \approx 1.05$ in^{21,22}). In line with expectation for the hysteretic behaviour of typical first-order ordering transitions, the transition back to

the ordered BCC-like state occurs at a temperature lower than the transition upon heating, i.e., $T_{\text{cool}} < T_{\text{melt}}$. The ordered structures obtained from this cooling process are slightly less ordered than those obtained by slowly heating up an initially perfect BCC lattice; this is evident in a very slight discrepancy in the energy value (which on the interval $kT \in [0.25, 0.8]$ is on average 0.116% higher than the energy values); it is even more evident in the structure factor which is sensitive to structural detail. The deviations are quantified by the τ order metric and shown on a logarithmic scale in Fig. 1.

The above findings obtained on systems that are cooled down or heated up are supported by 'isothermal simulations', that is, simulations at a fixed temperature with significantly longer simulation runs with 8.5×10^5 MD steps (as opposed to the 10^4 MD steps per temperature step in the cooling/melting simulations above).

The mean energies of these isothermal simulations, shown in fig. (1), support our earlier results. Four independent realisations of the system are simulated for each temperature as shown in the figure; data labelled 'isothermal melting' results from simulating a system from an initial BCC configuration, whereas 'isothermal freezing' refers to a system prepared from an initial ideal gas system; for further simulation details see Appendix VII C. The mean energy values of the isothermal simulations coincide largely with the energy trajectories of the slow cooling and heating processes, except in a small region around the order/disorder and disorder/order transitions. We thus conclude that the heating and cooling can be assumed a quasi static process except in the vicinity of the order/disorder and disorder/order transition.

The transitions (discontinuities) in the mean energy of the isothermal simulations are slightly offset from the values of the continuous cooling/heating transitions. The discontinuity of the mean energy of the isothermal heating systems occurs at a slightly lower temperature than all of the slowly heated systems; the discontinuity of the mean energy of the isothermal freezing systems occurs at a slightly higher value than the average transition temperature of the slowly cooled systems. This trend could indicate that our slowly cooled or heated systems are not quite fully equilibrated, but fairly close to equilibrium.

We note that the freezing isothermal systems show a similar spread of energy values after the disorder/order transition than the slowly cooled systems, indicating that the residual defects are not caused by too little equilibration time.

Our results (both for slow cooling/heating and for the isothermal simulations) are in good agreement with those from Ruscher's study²² of the Voronoi liquid. We add three comments in regards to the agreement:

(1) Ruscher's value for the melting temperature ($kT \approx 1.85$) is slightly lower than ours ($kT_m \approx 1.886$), and Ruscher's value for the freezing temperature ($kT_f \approx 1.05$) slightly higher than ours ($kT \approx 0.96$). These slight differences are probably due to our slightly faster cooling or heating rates, to the different system sizes and to slightly different thermostats and simulation parameters. (We note that, as expected for slower cooling rates, Ruscher finds a transition temperature for the isothermal melting which is slightly closer to the isothermal melting

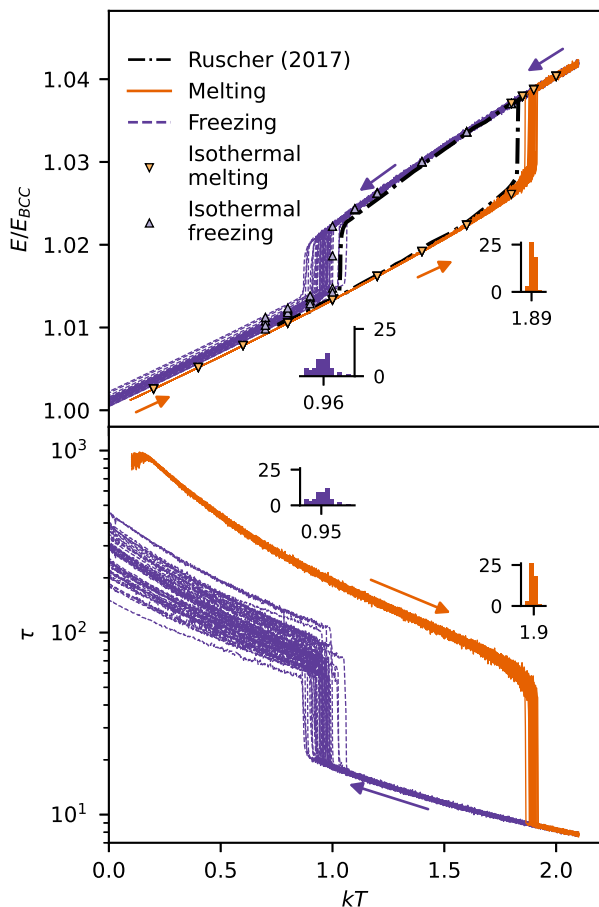


FIG. 1. Molecular dynamics (MD) simulation data of disorder-order (freezing) and order-disorder (melting) phase transitions of the Quantizer system observed at melting of a BCC crystal and freezing of an ideal gas, and comparison to earlier data by Ruscher²² (black dashed-dotted line). Shown is the energy (as per eq. 1, top panel) and τ order metric (as per eq. 4, bottom panel) of 48 individual runs for melting and freezing processes. The triangles in the top panel show the mean energy of isothermal systems run over a long time. All runs show a discontinuity in the energy and the τ order metric at the transition temperatures that are different for freezing and melting and which vary slightly from run to run. The insets show the distribution of the transition temperatures. Qualitatively the hysteresis between the temperature of the phase transition of the disorder/order (freezing) and order/disorder (melting) transitions described by Ruscher²² is reproduced. The ordered structure obtained by freezing shows variations from the BCC structure, which are most clearly visible in τ and which are indicative of residual defects in the structure. See Appendix VII C for simulation details.

system than ours. Within this systematic error due to slight differences in cooling/heating rates, we consider that our results agree with those of Ruscher.)

(2) At the finite size of our simulations ($N = 2000$ particles), we find a distribution for the values of the freezing temperature and the cooling temperatures which are (average \pm standard deviation) $kT_f = 0.96 \pm 0.04$ and $kT_m = 1.89 \pm 0.01$ for the MD simulations (1) and $kT_{freeze} = 0.97 \pm 0.03$ and $kT_{melt} = 1.886 \pm 0.006$ for the MC simulations (2). We under-

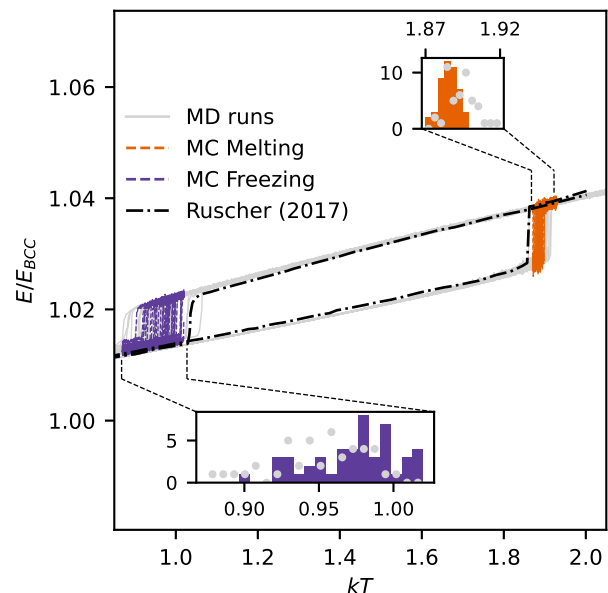


FIG. 2. Monte Carlo (MC) simulation data of disorder-order (freezing) and order-disorder (melting) phase transitions of the Quantizer system observed upon heating of a BCC crystal and cooling of an ideal gas. The plot shows 48 individual runs for melting and freezing (dashed, colored lines). The MC data is consistent with results from MD simulations, see Fig. 2, with slight differences in the variations of the transition temperatures; the MC melting runs show a slightly more narrow distribution of transition temperatures than the MD data, with $kT_m = 1.886 \pm 0.006$ and $kT_f = 0.97 \pm 0.03$, as seen in the insets showing the distribution of transition temperatures in colored bars and the MD data is indicated by light grey dots. See Appendix VII C for simulation details.

stand that Ruscher only presented data for a single simulation run with about 8000 particles.

(3) In our simulations, the final energy of the freezing curves differs slightly from that of the perfect BCC lattice. Visual examination shows that this is due to residual disordered artifacts in the otherwise ordered lattice. These deviations are more clearly visible in the τ parameter which is sensitive to small deviations from order.

Figure 2 shows Monte Carlo simulation data for the same system which are consistent with the Molecular Dynamics simulation data shown in Fig. 1, thereby providing further confirmation of these results. The quantitative values for the transition temperatures are consistent (within error bars) in MD and MC simulations; however, we observe a narrower spread of transition temperatures for the melting process in our MC simulations as compared to our MD simulations, see Tab. I.

This concludes our analysis of the quasi-static (slow) equilibrium cooling and heating of the Voronoi liquid. Confirming the results by Ruscher *et al.* we find the system to behave like a typical first-order order/disorder transition with hysteresis in that limit, with the low-temperature state given by the BCC lattice.

We now turn to a different question, namely that of what structures the Voronoi liquid adopts upon fast non-equilibrium

	kT_f	kT_m
Molecular dynamics	0.96 ± 0.04	1.89 ± 0.01
Monte Carlo	0.97 ± 0.03	1.886 ± 0.006
Ruscher ²²	1.05	1.85

TABLE I. Transition temperatures T_m for the order/disorder transition (melting) and T_f for the disorder/order (freezing) transition, as computed by molecular dynamics simulations, Monte Carlo simulations and as reported by Ruscher²². The notation is $T \pm \delta T$ where T is the average over all simulation runs and δT the standard deviation. The values for Ruscher’s data are estimates extracted from diagrams in her article²².

cooling or a quench. These data are obtained by MD simulations where the system is initialized in equilibrium configurations at high T , and then cooled at high cooling rates. The limit of an infinite cooling rate, where the temperature is abruptly set to 0, is here referred to as *quench*. These non-equilibrium final configurations are compared in particular to the structures obtained by Lloyd’s algorithm, discussed by Klatt *et al.*²³; Lloyd’s algorithm represents a steepest-descent minimization of the energy functional in eq. 1 and can therefore be regarded as a type of quench.

Figure 3 and Table II represent our analysis of the structure of the configurations that result from quenching the system, that is, by MD or MC simulations of a systems where a high-temperature ideal gas configuration evolves when the temperature is abruptly set to 0. Figure (3) shows the structure factors of the structures thus obtained and Table II the τ order metric calculated from these. See also Appendix VII A for a technical comparison of an MD quench and Lloyd’s algorithm.

These final structures are compared to the structures obtained by application of the (purely geometric) Lloyd’s algorithm to the same structures, as suggested by Klatt *et al.*²³ (and also to the data for that same system as reported by Klatt *et al.*²³). The key result is that, to a high degree of accuracy and within the statistical accuracy of our data, structures obtained by MD or MC quenches are indistinguishable from the converged Lloyd states in terms of the structure factor and the derived τ metric (within error bars).

Structural metrics for local order and local packing structure, namely the Minkowski structure metrics and cell statistics of the Voronoi tessellation, also show good agreement of the final structures of the different quenches. See Appendix VII B for further details. Moreover, we also find a hyperuniformity index H^{41} of the order of magnitude 10^{-4} .

Up to here, we have investigated the two extreme cases being (a) slow quasi-static heating and cooling (which leads to a hysteric order/disorder transition) and (b) quenching as the limit of maximally fast non-equilibrium cooling. We now turn our attention to the intermittent regime of cooling processes which are too fast to be quasi-static yet are not a quench.

The key result of Fig. 4 is that, upon rapid non-equilibrium cooling with sufficiently fast but finite cooling rates, the system tends to avoid a transition to an ordered (BCC) structure but instead converges to configurations that are similar in structure (as measured by the structure factor) and similar in energy values to the converged Lloyd states. If the cooling

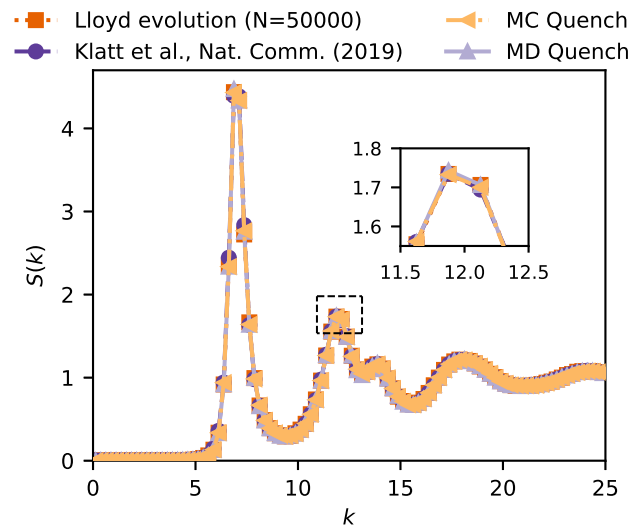


FIG. 3. Structure factor $S(k)$ of a quenched ideal gas (binomial point-process) at $kT = 0$ with $N = 2000$ particles and a particle density $\rho = 1$ using Molecular dynamics (MD), Monte Carlo (MC) and the gradient-descent-like Lloyd’s algorithm. Each structure factor is averaged over 24 individual runs. A detailed description of the processes and parameters are given in the method section II. All methods evolve into disordered structures with energies and values of the τ order metric equal within measurement uncertainties, see tab. (II). According to our data, these structures are identical to the universal, amorphous structures previously found by Klatt *et al.*²³ as remarkably stable, disordered minimal energy configurations of the Quantizer system. See Appendix VII C for simulation details.

is sufficiently fast, the value of the cooling rate only has a minor effect on the final structure that is reached at $kT = 0$; the remaining minor differences in energy are visible in the insert of Fig. 4 and are significantly smaller than the difference between the converged Lloyd states ($E/N = 118.82 \pm 0.02$) and that of the BCC crystal ($E/N = 117.815$).

For the fast cooling rates, the majority of the system do not show a phase transition. At a cooling rate of $-4 \cdot 10^{-3}$ none of the 24 runs showed a phase transition, out of the 24 runs at a cooling rate of $-8 \cdot 10^{-3}$ only one underwent a phase transition, and three out of 24 runs showed a phase transition at a cooling rate of $-4 \cdot 10^{-4}$. (These runs are omitted in the data shown here.)

Finally, we have analysed the slow quasi-static heating of a system that is prepared at $T = 0$ in converged Lloyd states. When heated slowly, the system energy gradually increases until a certain temperature following the same (or a very similar) curve to the rapid cooling cycles, in reverse. At a certain temperature (the value of which varies, potentially due to finite size effects), the energy jumps down to almost the energy of a BCC crystal being melted to the same temperature. When heated further, the system behaves similar to that of the melting curve of a system that started from a BCC crystal. There are small remnant differences in the energy (the purple curves in Fig. 4 are slightly above the orange curve) and the eventual transition to a disordered structure occurs at a slightly lower temperature. We do not know the exact nature of these slight

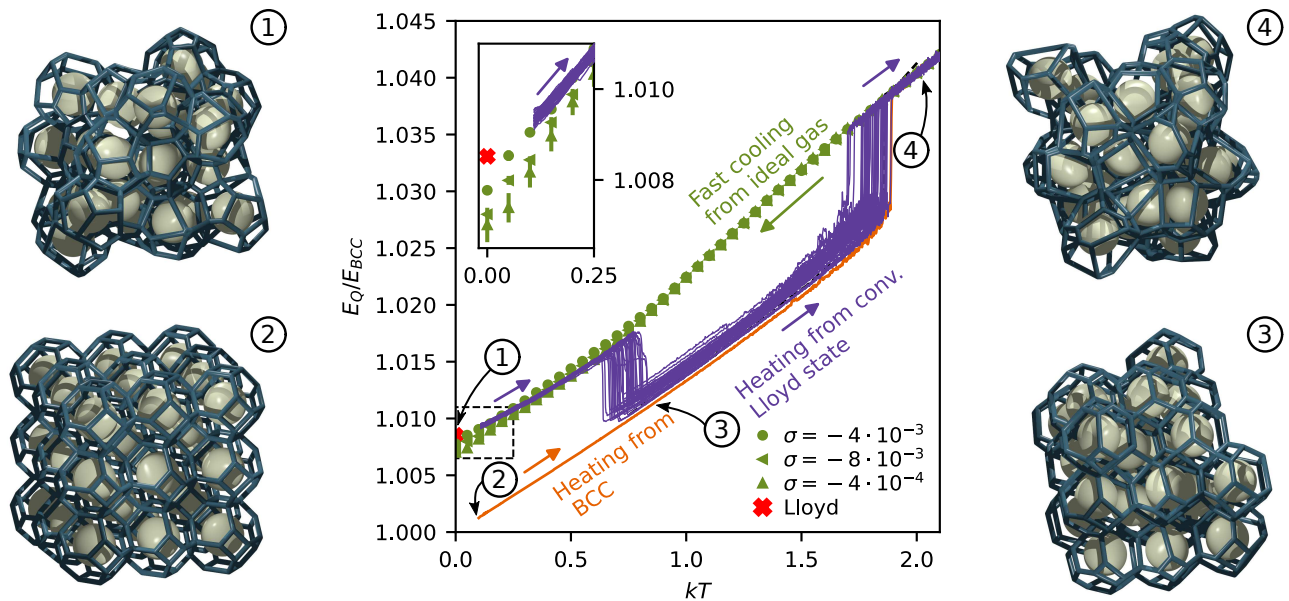


FIG. 4. Non-equilibrium cooling with a fast but finite cooling rate and slow equilibrium heating of the converged Lloyd states of Klatt *et al.*²³. The fast non-equilibrium cooling of a high-temperature ideal gas results in disordered structures very similar to the converged Lloyd states (dotted green curves). The dependence on the cooling rate σ is only weak for $|\sigma| > 4 \cdot 10^{-4} \varepsilon / \delta$ (see inset). Upon cooling, the energy initially follows the same functional form as for a slow equilibrium cooling, however it fails to show any sign of the ordering transition (which the slowly cooled systems undergo for $kT_{melt} \approx 0.96$). When, from small T , the converged Lloyd states are heated slowly at $\sigma = 2.5 \times 10^{-4}$ (purple curves), they initially show at $kT \approx 0.74 \pm 0.05$ a transition to a (softened) BCC configuration which then melts at a slightly lower phase transition temperature at $kT'_m \approx 1.80 \pm 0.04$. The orange curve represents the slow equilibrium melting transition starting from a low-temperature BCC phase. All data shown here is obtained by Molecular Dynamics simulations. See Appendix VII C for simulation details. On the left and right hand side, we show snapshots taken from MD simulations.

differences. The degree of residual randomness in these intermediate BCC-like states appears to facilitate a melting transition at a slightly lower temperature.

The “drop” to a BCC-like states can be avoided, when a system prepared as a converged Lloyd state at $T = 0$ is quickly heated. At a heating rate of $\sigma \approx 9.3 \cdot 10^{-3}$ all out of 24 individual runs avoid the intermediate BCC-like state and follow the curve of a quickly cooled system up to the liquid state. With decreasing heating rates the systems get more likely to fall back into the intermediate states: at a heating rate of $\sigma \approx 4.3 \cdot 10^{-3}$ 6 out of 24 runs return to the BCC like state. This behavior while heating is analog to the freezing case: here too the BCC ground state can be avoided if the system is cooled very quickly.

IV. CONCLUSION

We have studied the configuration of many-particle system that are formed by the many-body interaction of the Quantizer energy^{16,17,31}, that is, of the Voronoi liquid²¹. We confirmed the freezing and melting transitions found by Ruscher, Baschnagel, and Farago²¹ using both MD and MC simulations. A slow cooling in equilibrium leads to the formation of BCC crystallites, as expected, since the conjectured ground state (at $T = 0$) is the BCC lattice.

In contrast, a quench from high temperature states leads to

	E/E_{BCC}	τ
MD Quench	1.00844 ± 0.00002	33 ± 1
MC Quench	1.00854 ± 0.00003	33 ± 1
Lloyd's Iteration	1.00852 ± 0.00003	33 ± 1
Klatt <i>et al.</i> ²³	1.008 ± 0.001	32 ± 1

TABLE II. Final energies and τ values of quenched ideal gas systems as described in fig. (3). The τ order metric measures the degree of order in the system, it diverges for crystalline structures and is zero for complete spatial randomness. The value of the τ order metric from Klatt *et al.*²³ is that for configurations from Binomial point-processes (from Table 2 in the supplementary information); here, we added systematic errors discussed both in Klatt *et al.*²³ and our method section. See Appendix VII C for simulation details.

disordered amorphous structures, more similar to the amorphous states found by the Lloyd's algorithm²³. A finite cooling rate results in final energies slightly below that of the final state of Lloyd's algorithm, but as we increase the cooling rate the final energies increase. A quench at $T = 0$ leads to final states whose energies, two-point statistics and local multi-point statistics coincides within our statistical accuracy with those of the converged Lloyd states.

To explain both the similarities and differences between a fast MD quench and the Lloyd's algorithm, we derive a limit in which a modified MD quench, where the mass of a particle is given by the volume of its cell, coincides with the iterations

of the Lloyd algorithm.

Melting the amorphous converged Lloyd states, we find that the system remains on the amorphous branch for a finite range of temperatures (before the system returns to crystalline branch), which agrees with the meta-stability of the converged Lloyd states.

In future work, MC simulations of the ‘‘Quantizer problem’’ (i.e., Voronoi liquid) make it possible to determine the density of states (e.g., using the Wang-Landau algorithm⁴²) to further study the intriguing energy landscape of this many-particle interaction.

Lloyd’s algorithm is a gradient-descent minimization method tailored to the Quantizer problem, in the following sense: The displacement of each point into the direction of the center of mass of its Voronoi cell corresponds to the direction of the negative gradient. Further, the displacement into the center of mass of the Voronoi cell (rather than just in that direction), provides a ‘local optimum displacement’ for the individual cell. The question arises naturally what final structures are obtained when applying other energy minimization methods such as the conjugate gradient descent method, BFGS or others. Preliminary results indicate, that conjugate gradient methods, steepest descent as well as BFGS minimization methods as implemented in the GSL⁴³ seem to evolve random initial structures into amorphous structures that are very similar to the inherent structure found by Lloyd’s algorithm (Note that these algorithms were provided with the gradient direction from Lloyd’s algorithm, as a closed formula for the gradient of the energy functional is not available.) A quantitative statistical analysis needs to include a detailed analysis of the observed cases where the minimization methods get stuck in seemingly shallow local minima, and is beyond the scope of this article.

Ultimately, the research presented in this article supports the search for disordered ground states and long-lived inherent structures that offer novel physical properties due to their isotropy (in contrast to their crystalline counter parts). A key question for experimental realizations is the role of long- and short-range interaction in such systems.

V. ACKNOWLEDGEMENTS

We are grateful to Massimo Ciamarra who pointed us towards the work of Ruscher and colleagues on the Voronoi Liquid. We thank Salvatore Torquato for discussions and helpful comments, and we thank Jorg Baschnagel, Jean Farago, and Celine Ruscher for helpful comments and interesting questions. This work was supported in part by the Princeton University Innovation Fund for New Ideas in the Natural Sciences. This work was supported by resources provided by the Pawsey Supercomputing Centre with funding from the Australian Government and the Government of Western Australia, as well as LUNRAC at Lund, Sweden.

VI. DATA AND CODE AVAILABILITY

The data that support the findings of this study and the code used to generate them are available from the corresponding author upon request.

VII. APPENDIX: ALGORITHMIC EQUIVALENCY, ADDITIONAL STRUCTURE METRICS, AND SIMULATION DETAILS

A. Lloyd’s algorithm as a limit of an MD quench

We showed that a fast MD quench results in a structure similar to the converged Lloyd states. Here we discuss the conditions under which an MD quench collapses to a ‘Lloyd quench’. MD simulations compute the time evolution of particles, where each step advances time by an increment Δt , thus the position of the i -th particle at time t , given by $\mathbf{r}_i(t)$, is equivalent to $\mathbf{r}_i(n\Delta t) =: \mathbf{r}_{i,n}$.

Since Lloyd’s algorithm is missing an intrinsic definition of a time scale, a Lloyd quench can only be compared to an MD quench on a step by step basis. The position of the i -th particle at step n is denoted by $\mathbf{r}_{i,n}$. A single Lloyd’s iteration is then given by $\mathbf{r}_{i,n+1} = \mathbf{c}_{i,n}$, where $\mathbf{c}_{i,n}$ is the centroid of the Voronoi cell associated to the i -th particle at step n .

The position of the i -th particle after one MD step of time length Δt is given by $\mathbf{r}_{i,n+1} = \mathbf{r}_i(t + \Delta t)$ which can be approximated by its Taylor series

$$\mathbf{r}_{i,n+1} = \mathbf{r}_{i,n} + \dot{\mathbf{r}}_{i,n}\Delta t + \frac{(\Delta t)^2}{2}\ddot{\mathbf{r}}_{i,n} + \text{higher orders} \quad (5)$$

where a dot denotes the time derivative: $\dot{\mathbf{r}} = \frac{\partial}{\partial t}\mathbf{r}$. The force acting on particle i is given as $\ddot{\mathbf{r}}_i = \frac{\mathbf{F}_i}{m_i} = \gamma \frac{V_i}{m_i}(\mathbf{c}_i - \mathbf{r}_i)$. Substitute into eq. 5 yields

$$\mathbf{r}_{i,n} = \left(1 - \frac{\gamma V_i (\Delta t)^2}{m_i}\right) \mathbf{r}_{i,n} + \left(\frac{\gamma V_i (\Delta t)^2}{m_i}\right) \mathbf{c}_{i,n} + \dot{\mathbf{r}}_{i,n}$$

where we neglect orders higher than second derivative. For an MD step being equivalent to a Lloyd iteration $\mathbf{r}_i(t + \Delta t) = \mathbf{c}_i$ must hold. Thus, the time step Δt must be chosen as

$$\Delta t = \sqrt{\frac{2 m_i}{\gamma V_i}}$$

For this equation to hold, the masses of all particles must be set equal their volume before each simulation step. The temperatures are set to zero after each simulation step, this acts as a thermostat simulating a quench. In this limit an MD step is equivalent to a Lloyd iteration.

On the one hand, this limit demonstrates similarities of Lloyd’s algorithm and a quench for Voronoi tessellations with energies close to the ground state (with a sharp cell volume distribution). On the other hand, the analysis reveals subtle differences that may lead to a slightly different energies and (global) structures.

B. Local structure metrics

Structures can be locally characterized using the so-called Minkowski metrics^{24,36}. These define several scalar, vectorial and tensorial quantities measuring the shape of a convex body K such as a Voronoi cell. Here we specifically employ the surface Minkowski tensors $W_1^{0,s}$ describing the radial distribution of outer normal vectors of K ²³. It can be conveniently decomposed into spherical harmonics

$$\rho_s^m(K) = \sqrt{\frac{4\pi}{2s+1}} \frac{\sum_k A_k Y_s^m(\mathbf{n}_k)}{\sum_k A_k}$$

where A_k are the surface areas of the faces of the body K and \mathbf{n}_k the outer normal vectors. From this tensor rotational invariants can be constructed:

$$q_s(K) := \sum_{m=-s}^s |\rho_s^m(K)|^2$$

These q_s describe the shape of a cell independent of its size and orientation and thus can be used as a shape metric. Here we compute the quantities $q_{2,4,5,6,8}$ for each cell in a system and show their normalized distribution.

The distribution of the number of edges of faces as well as the number of faces of each cells in the Voronoi tessellation is presented as a further measurement of the local packing.

Our results are shown in fig. (5) and fig. (6). We present the shape metrics and Voronoi cell statistics for the final structures obtained MC, MD and Lloyd quenches, as well as fast cooling MD simulations. For each quench type the distribution is averaged over 24 individual simulation runs. The data shows good agreement within statistical limits of the distributions of the MD, MC and Lloyd quenches. These findings further support the equality of the final structures, as previously indicated by equal energies as well as τ values.

The distributions of the final structures obtained by quickly cooled systems, however, show significant differences compared to the quenched structures. A clear trend is visible: the higher the (absolute value of the) cooling rate the higher the deviation from the inherent structure. This is visible in the Minkowski structure metrics, but even more in the Voronoi statistics. These results are in line with a similar trend in the final energies, which decrease - hinting towards more optimal structures - with increasing heating rates.

C. Simulation parameters

Quenches, fig. (3), table (II) All initial configurations are binomial point processes (ideal gases) with $N = 2000$ and $\rho = 1$. The structure factors, τ and energy values of MC, MD and Lloyd's algorithm runs are averaged over 24 individual runs. **MD:** MD step size chosen as $\Delta t = 0.005$, initial temperature set to $kT = 2.1$. An initial set of 5000 MD steps are performed at $kT = 2.1$ to equilibrate the initial configuration,

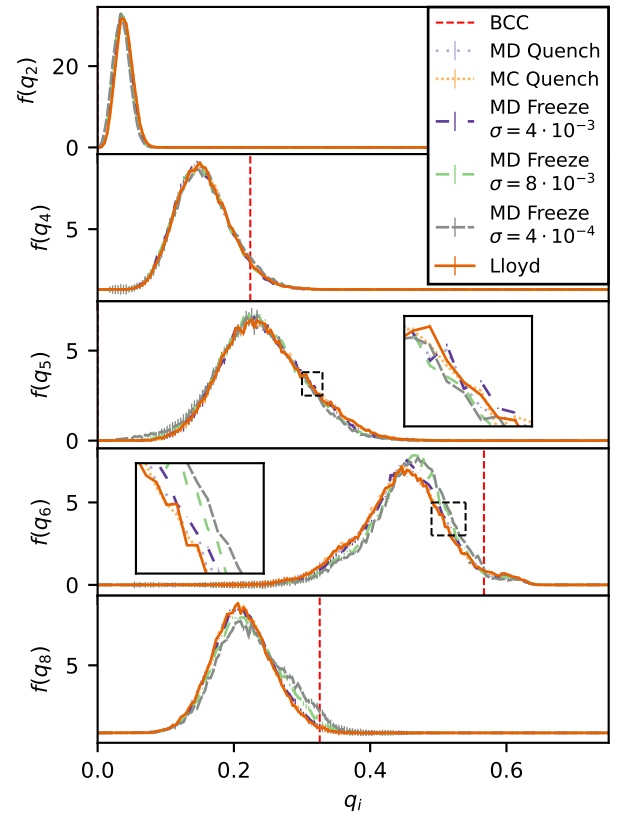


FIG. 5. Local order and structure measures of final structure obtained by MD, MC and Lloyd quenches, as well as fast freezing MD simulations. Shown are the rotational invariants $q_{2,4,5,6,8}$ of the face-normal Minkowski tensors. These robust and sensitive measures characterise the shape of single Voronoi cells and thus local order and structure of the systems. The values of a BCC shaped cell is shown for reference. The data shows good agreement of the final structures of MD, MC and Lloyd quenches within statistical uncertainties indicating that the final structures of the MD and MC quenches are identical to the ones of the Lloyd quench. The fast freezing MD simulations show good agreement in q_2 and q_4 , however, increasing differences in q_5, q_6 and q_8 with increasing cooling rate, indicating a differences in the local order compared to the structures obtained by the quenches. These findings are in line with the decreasing energies of the final structures with increasing cooling rates.

then the temperature is set to $kT = 0$ and the system is run for 6×10^5 MD steps. **MC:** Immediately after initialization temperature is set to $kT = 0$, then a total of 8.1×10^8 MC steps are run. Step size is adapted every 3×10^7 steps. **Lloyd's algorithm:** A total of 50000 steps are run. While the τ value in table (II) was taken from the supplementary material from²³, the structure factor shown in fig. (3) was generated by us from the dataset 3D-FINAL-CONFIGURATION-DERIVED-FROM-BINOMIAL-PP-1.DAT provided by Klatt *et al.*²³. All structure factors are computed with a bin width of 0.25 and a cutoff $k_{\max} = 25$.

MD melting/freezing, fig. (1) 48 individual runs for each melting and freezing were run. **Melting** runs were initialized as BCC lattices, with each component of the velocities randomly drawn from a normal distribution to match a system

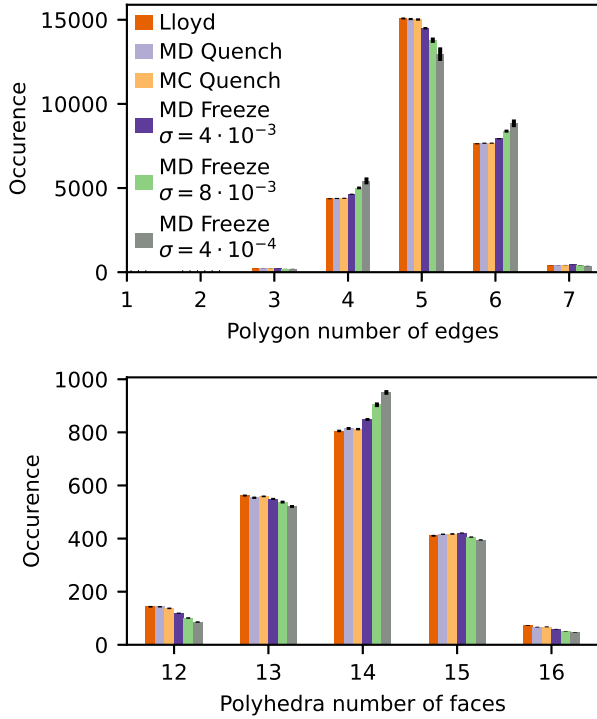


FIG. 6. Cell and face order distributions of the Voronoi cells in the structures obtained by MD, MC and Lloyd quenches as well as fast frozen MD simulations. Shown is the number of faces with n edges (top) and the number of cells with n faces in the Voronoi tessellation of the final structures. The data shows good agreement within statistical limits of the MD, MC and Lloyd quenches, where as the fast freezing MD runs show significant deviations increasing with increasing cooling rate.

temperature of $kT = 0.1$. The velocities are modified so the center of mass of the system is at rest. The initial thermostat temperature is set to $kT = 0.1$. **Freezing** runs were initialized as ideal gas, thus each position component randomly chosen to uniformly cover the simulation box with random velocities matching an initial temperature of $kT = 2.1$ with the center of mass of the system at rest. For both melting and freezing runs the thermostat is initialised with $Q = 20$, $s = 1$ and $\dot{s} = 1$, the MD time step is chosen as $\Delta t = 0.001$. All systems ran a set of 5×10^5 initial relax steps to equilibrate the system and thermostat at the respective initial temperature. Then 800 (melting)/840 (freezing) temperature steps, each with an increment of $\Delta kT = \pm 2.5 \times 10^{-3}$ are run, resulting in a cooling rate of $\sigma = \frac{2.5 \times 10^{-3} \epsilon}{10000 \cdot 0.001 \delta} = 2.5 \times 10^{-4} \epsilon / \delta$. For each temperature, 10000 MD relax steps are run followed by a measurement phase comprising 1500 MD steps where every 25 steps the energy and structure factor is measured. For the isotherms 4 runs at each temperature for each freezing and melting systems are run. The particles in melting systems are initialized on a BCC lattice with velocities drawn from a normal distribution to match their respective temperature with a resting center of mass. The initial positions of the particles in the isothermal freezing systems are uniformly distributed over the simulation box with velocities drawn from a normal

distribution to match their respective temperature (ideal gas). Both melting and freezing isothermal systems are then run for $8.5 \cdot 10^5$ steps with a time step of $\Delta t = 0.001$. The thermostat is initialized with $Q = 20$, $s = 1$ and $\dot{s} = 1$. The mean energies are averaged over the last $1.7 \cdot 10^5$ steps.

MC melting/freezing, fig. (2) Since MD simulations outperforms MC code by far, we used MD simulations to generate initial configurations very close to the phase transition region and then continued these runs with MC code. The parameters for the MD runs are identical to the ones mentioned above with these exceptions: no initial relax steps are performed, the positions of the particles in the systems initialized as ideal gas are identical across all systems, however, do have randomly chosen velocities. The in total 48 runs were given different initial thermostat settings, where two runs shared one of the combinations between $Q \in \{60, 50, 40, 30, 20, 10\}$ and $(s, \dot{s}) \in \{(0.2, 0), (1, 0.5), (1.5, 1), (4, 3)\}$. Only 500 measure steps were performed at each temperature. The initial configurations for the MC runs were taken after the relax phase at $kT = 1.87$ (melting) and $kT = 1.02$ (freezing). A total of 213 (melting)/320 (freezing) temperature increments each with $\Delta kT = \pm 4.7 \times 10^{-4}$ were simulated. At each temperature a total of 6×10^6 MC relax steps were performed, followed by 3.8×10^4 measurement steps, with 2000 MC steps in between individual measurements.

Melting of the converged Lloyd states, fig. (4) The 48 individual MD simulations are initialized with converged Lloyd states, thus $N = 2000$ and $\rho = 1$. Random temperatures are assigned to match an initial temperature $kT = 0.05$ with the center of mass of the system at rest. 2×10^5 initial relax steps are performed. Thermostat is initialized with $Q = 20$ and $s = \dot{s} = 1$. MD time step is chosen as $\Delta t = 0.001$. A total of 840 temperature increments with $\Delta kT = 2.5 \times 10^{-3}$ are computed. Each temperature has 10000 relax steps and 1500 measurements steps with 25 steps in between individual measurements. All data represented by symbols are MD simulations initialized as ideal gas, with random velocities matching their initial temperatures, with the center of mass at rest. All ran a set of initial relax steps of 20000 MD steps, had 2400 relax and 100 measurement MD steps for each temperature increment, with 25 MD steps between each measurement. The olive circles (“ $\sigma = -4 \cdot 10^{-3}$ ”) is combined data from 10 sets, each set consisting of 24 averaged runs, starting at different initial temperatures $kT = (2.5, 2.55, 2.6, 2.65, 2.7, 2.75, 2.8, 2.85, 2.9, 2.95)$. Each set had six temperature increments of $\Delta kT = -0.5$. Combining the interlaced sets yields the curve as shown. The same was done for the olive triangles (“ $\sigma = -8 \cdot 10^{-3}$ ”), however, only 2 sets (each averaging over 24 runs) started at $kT = (2.1, 2.15)$ and had 22 temperature increments with $\Delta kT = -0.1$. The olive pyramids (“ $\sigma = -4 \cdot 10^{-4}$ ”) is a single set averaging over 24 runs starting at $kT = 2.1$ with 43 temperature increments with $\Delta kT = -0.05$.

¹D. Weaire and R. Phelan, *Philos. Mag. Lett.* **69**, 107 (1994).

²D. Weaire, *The Kelvin Problem* (Taylor & Francis, London, 1997).

³T. Hales, *Ann. Math.* **162**, 1065 (2005).

⁴S. Torquato, G. Zhang, and F. H. Stillinger, *Phys. Rev. X* **5**, 021020 (2015).

- ⁵G. Zhang, F. H. Stillinger, and S. Torquato, Phys. Rev. E **92**, 022119 (2015).
- ⁶G. Zhang, F. H. Stillinger, and S. Torquato, Phys. Rev. E **92**, 022120 (2015).
- ⁷G. Zhang, F. H. Stillinger, and S. Torquato, Soft Matter **13**, 6197 (2017).
- ⁸S. Ghosh and J. L. Lebowitz, Commun. Math. Phys. **363**, 97 (2018).
- ⁹G. Zhang, F. H. Stillinger, and S. Torquato, Sci. Rep. **6**, 36963 (2016).
- ¹⁰D. Bi, J. H. Lopez, J. M. Schwarz, and M. L. Manning, Nat. Phys. **11**, 1074 (2015).
- ¹¹M. Merkel and M. L. Manning, New J. Phys. **20**, 022002 (2018).
- ¹²A. Gersho, IEEE Trans. Inf. Theory **25**, 373 (1979).
- ¹³S. Lloyd, IEEE Trans. Inf. Theory **28**, 129 (1982).
- ¹⁴J. Conway and N. J. A. Sloane, *Sphere Packings, Lattices and Groups*, 3rd ed., Grundlehren Der Mathematischen Wissenschaften (Springer-Verlag, New York, 1999).
- ¹⁵A. Okabe, B. Boots, K. Sugihara, and S. N. Chiu, *Spatial Tessellations: Concepts and Applications of Voronoi Diagrams*, 2nd ed. (Wiley, Chichester; New York, 2000).
- ¹⁶Q. Du and D. Wang, Comput. Math. Appl. **49**, 1355 (2005).
- ¹⁷Q. Du, M. Gunzburger, and L. Ju, Numer Math Theor Meth Appl **3**, 119 (2010).
- ¹⁸R. Gray, IEEE ASSP Mag. **1**, 4 (1984).
- ¹⁹L. Lu, F. Sun, H. Pan, and W. Wang, IEEE Trans. Vis. Comput. Graph. **18**, 1880 (2012).
- ²⁰S. Torquato, Phys. Rev. E **82** (2010), 10.1103/PhysRevE.82.056109.
- ²¹C. Ruscher, J. Baschnagel, and J. Farago, EPL **112**, 66003 (2015).
- ²²C. Ruscher, *The Voronoi Liquid : A New Model to Probe the Glass Transition*, PhD thesis, École doctorale Physique et chimie-physique (2017).
- ²³M. A. Klatt, J. Lovrić, D. Chen, S. C. Kapfer, F. M. Schaller, P. W. A. Schönhöfer, B. S. Gardiner, A.-S. Smith, G. E. Schröder-Turk, and S. Torquato, Nat. Commun. **10**, 811 (2019).
- ²⁴G. E. Schröder-Turk, W. Mickel, S. C. Kapfer, M. A. Klatt, F. M. Schaller, M. J. F. Hoffmann, N. Kleppmann, P. Armstrong, A. Inayat, D. Hug, M. Reichelsdorfer, W. Peukert, W. Schwieger, and K. Mecke, Adv. Mater. **23**, 2535 (2011).
- ²⁵W. Thomson, Acta Math. **11**, 121 (1887).
- ²⁶C. Ruscher, J. Baschnagel, and J. Farago, Phys. Rev. E **97**, 032132 (2018).
- ²⁷C. Ruscher, A. N. Semenov, J. Baschnagel, and J. Farago, J. Chem. Phys. **146**, 144502 (2017).
- ²⁸C. Ruscher, S. Ciarella, C. Luo, L. M. C. Janssen, J. Farago, and J. Baschnagel, J. Phys.: Condens. Matter **33**, 064001 (2020).
- ²⁹S. Torquato and F. H. Stillinger, Phys. Rev. E **68**, 041113 (2003).
- ³⁰S. Ghosh and J. L. Lebowitz, Indian J. Pure Appl. Math. **48**, 609 (2017).
- ³¹S. Torquato, Phys. Rep. **745**, 1 (2018).
- ³²S. Atkinson, G. Zhang, A. B. Hopkins, and S. Torquato, Phys. Rev. E **94**, 012902 (2016).
- ³³N. Metropolis, A. W. Rosenbluth, M. N. Rosenbluth, A. H. Teller, and E. Teller, J. Chem. Phys. **21**, 1087 (1953).
- ³⁴B. Krüger and J. F. Knauf, “Mocasinns,” (2016).
- ³⁵B. Krüger, *Simulating Triangulations: Graphs, Manifolds and (Quantum) Spacetime*, Doctoralthesis, FAU University Press (2016).
- ³⁶G. E. Schröder-Turk, W. Mickel, S. C. Kapfer, F. M. Schaller, B. Breidenbach, D. Hug, and K. Mecke, New J. Phys. **15**, 083028 (2013).
- ³⁷C. H. Rycroft, Chaos **19**, 041111 (2009).
- ³⁸S. Nosé, Mol. Phys. **100**, 191 (1983).
- ³⁹G. J. Martyna, D. J. Tobias, and M. L. Klein, J. Chem. Phys. **101**, 4177 (1994).
- ⁴⁰J.-P. Hansen and I. R. McDonald, *Theory of Simple Liquids: With Applications to Soft Matter*, 4th ed. (Academic Press, Amsterdam; Boston, 2013).
- ⁴¹We estimate H by fitting a Gaussian-shaped density to the peak ($6 < k < 7.5$) and by extrapolating a second-degree polynomial $ax^2 + c$ to the origin ($k_{\min} < k < 4$). The precise value of H depends on the fit range and functional form.
- ⁴²F. Wang and D. P. Landau, Phys. Rev. Lett. **86**, 2050 (2001).
- ⁴³See <https://www.gnu.org/software/gsl/> for details on the implementation of the minimization methods and further information.